

Microtubule Dynamics Are Necessary for Src Family Kinase-Dependent Growth Cone Steering

Daniel M. Suter,¹ Andrew W. Schaefer,
and Paul Forscher*

Department of Molecular, Cellular,
and Developmental Biology
Yale University
P.O. Box 208103
New Haven, Connecticut 06520

Summary

Dynamic microtubules explore the peripheral (P) growth cone domain using F actin bundles as polymerization guides [1, 2]. Microtubule dynamics are necessary for growth cone guidance [3–6]; however, mechanisms of microtubule reorganization during growth cone turning [7–9] are not well understood. Here, we address these issues by analyzing growth cone steering events *in vitro*, evoked by beads derivatized with the Ig superfamily cell adhesion protein apCAM. Pharmacological inhibition of microtubule assembly with low doses of taxol or vinblastine resulted in rapid clearance of microtubules from the P domain with little effect on central (C) axonal microtubules or actin-based motility. Early during target interactions, we detected F actin assembly and activated Src, but few microtubules, at apCAM bead binding sites. The majority of microtubules extended toward bead targets after F actin flow attenuation occurred. Microtubule extension during growth cone steering responses was strongly suppressed by dampening microtubule dynamics with low doses of taxol or vinblastine. These treatments also inhibited growth cone turning responses, as well as focal actin assembly and accumulation of active Src at bead binding sites. These results suggest that dynamic microtubules carry signals involved in regulating Src-dependent apCAM adhesion complexes involved in growth cone steering.

Results and Discussion

Dynamic Microtubules Efficiently Explore the Peripheral Domain over Time

Previous studies suggest that microtubule-actin filament “cross-talk” is critical for growth cone guidance [3–6, 8, 10, 11], but the underlying mechanisms are not clear. Using multimode fluorescent speckle microscopy (FSM), we recently showed that microtubules interact closely with filopodial F actin bundles, which serve not only as guides for microtubule assembly into the growth cone P domain, but also transport microtubules rearward by retrograde actin flow [2]. This process promotes constant exploration of the P domain and rapid microtu-

bule turnover, but the functional implications of this process have not been reported.

To characterize the spatial characteristics of microtubule exploration, we quantified microtubule extensions beyond a boundary set at 75% of the width of the P domain (Figures 1A–1D). Whereas a snapshot (Figure 1A) catches a few microtubules passing this criterion (arrowheads), integrating microtubule behavior over 10 min reveals that microtubules stochastically explore essentially the entire P domain (Figure 1B; see also Supplemental Movie 1 at <http://www.current-biology.com/cgi/content/full/14/13/1194/DC1>). Interestingly, P domain sampling appears to be somewhat region dependent (Figures 1C and 1D), with more frequent long microtubule extensions on the sides of the growth cone than distally along the axis of growth. Histograms of microtubule extensions for an individual growth cone over a 10 min period and for a population are shown in Figures 1C and 1D, respectively. The lower density of long-lived distal microtubule extensions along the axis of growth appears to be due to spatial differences in rates of retrograde actin flow. Specifically, actin flow rates were about 15% higher in the distal quadrants than on the sides of growth cones (Figure 1D). Since microtubules are coupled to retrograde flow >65% of the time [2], this probably negatively biases microtubule extension in the distal quadrants. Alternatively, spatial differences in microtubule assembly dynamics could be present; however, no evidence of this was observed (unpublished observations). These results suggest the possibility of regional differences in sensory potential—perhaps enhanced microtubule exploration on growth cone sides enhances peripheral target detection.

Given that retrograde actin flow transports microtubules out of the P domain at about the same rate as they assemble [2], factors that pause microtubule assembly should result in rapid clearance of microtubules from the P domain. To test this prediction, we dampened microtubule dynamics using either vinblastine (25 nM) or taxol (100 nM) at doses known to block assembly with minimal effects on microtubule structural integrity or polymer mass [3, 12]. Both of these treatments resulted in clearance of dynamic microtubules from the P domain, without disrupting microtubule structure in the C domain or significant alteration of peripheral actin filament organization (Figures 1F–1H) or retrograde actin flow (Figure 1E). To analyze the mechanism of this microtubule clearance, we visualized microtubule dynamics with FSM before and after drug treatment. Taxol application caused microtubules to undergo long pauses in their assembly (Figures 1I and 1J; see Supplemental Movie 2). When microtubule assembly rates were less than retrograde actin flow, microtubules were transported out of the P domain at about the rate of retrograde actin flow (Figure 1K; Supplemental Movie 3). Note that the microtubule tip appeared to remain attached to a moving filopodial actin bundle (arrowhead), while the more proximal microtubule segment detached and formed a loop, suggesting the presence of a microtubule-actin

*Correspondence: paul.forscher@yale.edu

¹Present address: Department of Biological Sciences, Purdue University, Lilly Hall 2-239, 915 West State Street, West Lafayette, Indiana 47907.

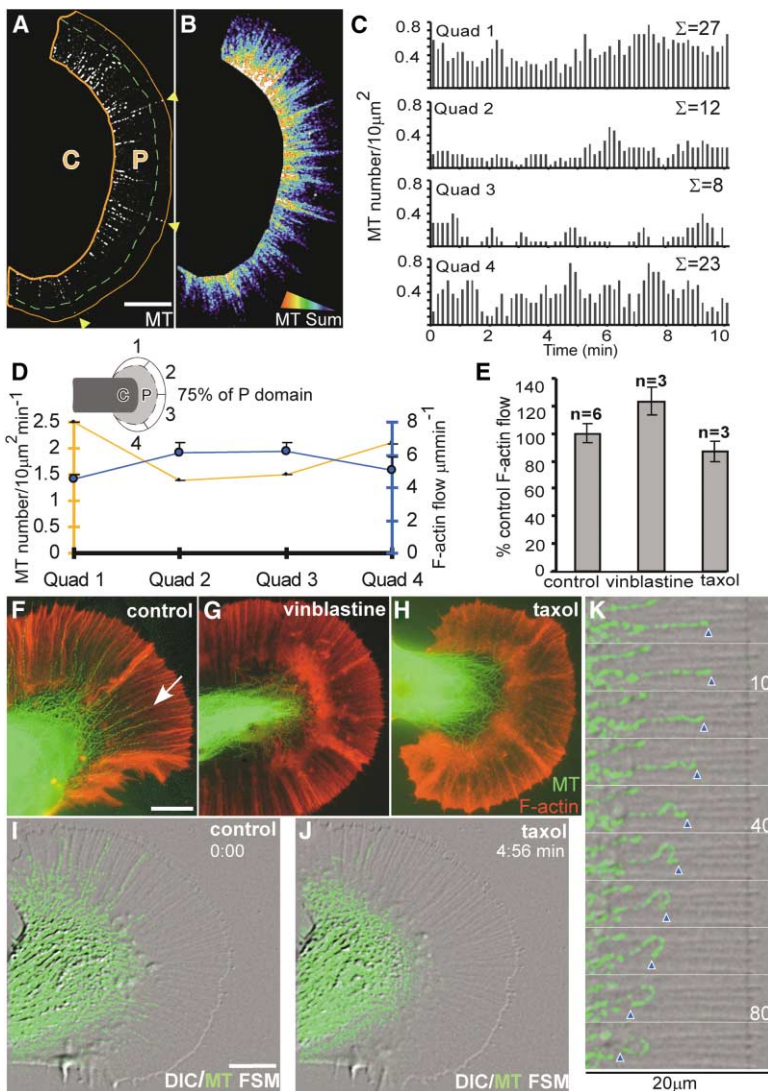


Figure 1. Dynamic Microtubules Efficiently Interrogate P Domain Space over Time

(A) P domain microtubule distribution at a single time point visualized by FSM in a live growth cone. The P domain is outlined by an orange line; hatched green line represents distal 75% border.

(B) Microtubule density in P domain summed over 10 min. Images taken every 10 s were binarized and summed.

(C) Microtubule densities past the 75% border plotted against time in quadrants (see inset in D) for a single growth cone.

(D) Plot showing that the average microtubule density (mean + SEM from 6 growth cones) over time in the distal P domain is inversely correlated with retrograde actin flow.

(E) Actin flow rates measured with bead markers under control conditions and after 20 min in 25 nM vinblastine or 100 nM taxol were not significantly different (mean values ± SEM [n = experiments], normalized by control flow rates, t test; p > 0.05).

(F–H) Immunocytochemistry of microtubule (green) and actin filament (red) distribution in growth cones: control (F); after 20 min in 25 nM vinblastine (G) or 100 nM taxol (H). Microtubules normally extend into P domain along actin bundles (arrow in F) but are absent from P domain after dampening microtubule dynamics.

(I and J) Multimode FSM (DIC/microtubule dynamics) before (I) and after (J) taxol treatment. (K) Time-lapse montage (10 s intervals) of microtubule immediately after taxol addition; microtubule plus end marked by blue triangle. Microtubule was transported at 4.5 μm min⁻¹. Scale bars equal 10 μm.

Supplemental Movie 1 shows DIC/MT visualization of a different control growth cone. Supplemental Movie 2 shows DIC/MT visualization of the taxol-treated growth cone from (J). Supplemental Movie 3 shows DIC/MT visualization of the individual MT in taxol shown in (K).

filament binding complex near the microtubule plus end. Low doses of vinblastine had similar effects (data not shown).

F Actin, Active Src, and Few Microtubules Localize Early at Bead Target Sites

We were interested in whether the microtubule exploration of the P domain described above could be involved in signaling, as suggested in the context of directed cell motility and morphogenesis [13] and in regulation of focal adhesion turnover [14, 15]. To address this, we used the previously described restrained bead target interaction assay (RBI) [16]. Beads coated with a recombinant version of the Ig superfamily cell adhesion molecule, apCAM, (Supplemental Figure S1) or 4E8 (an apCAM-specific monoclonal antibody) elicit growth cone turning responses involving focal actin assembly, slowing of retrograde actin flow, and C domain and microtubule advance toward targets [16]. These responses also depend on recruitment of active Src family tyrosine kinase (henceforth termed “Src”) at bead contact sites [17]; however, the relationship between focal actin as-

sembly, microtubule advance, retrograde flow, and the Src kinase activity during turning responses has not been reported.

To address these issues, interactions were halted by fixation at various time points, followed by immunolocalization of microtubules, actin filaments, and activated Src. During the “latency period,” defined as after bead placement but before C domain and leading edge advance (Figures 2A and 2B), microtubule distributions were similar to control growth cones (Figures 2C, 2H, and 1F) with no significant accumulation of microtubules near bead binding sites. In cells fixed during the latency period, an average of 0.8 microtubules were observed near beads (Figure 2I). Note that this number significantly underestimates actual microtubule activity at bead targets, since a bead will typically experience 15–25 microtubule explorations during a ~10 min latency period (Figures 1C and 1D). Contrasting with the lack of microtubule accumulation, F actin around restrained beads increased more than 300% (Figures 2D, open arrow, and 3F) during the latency period. In addition, when active Src distribution was assessed using a

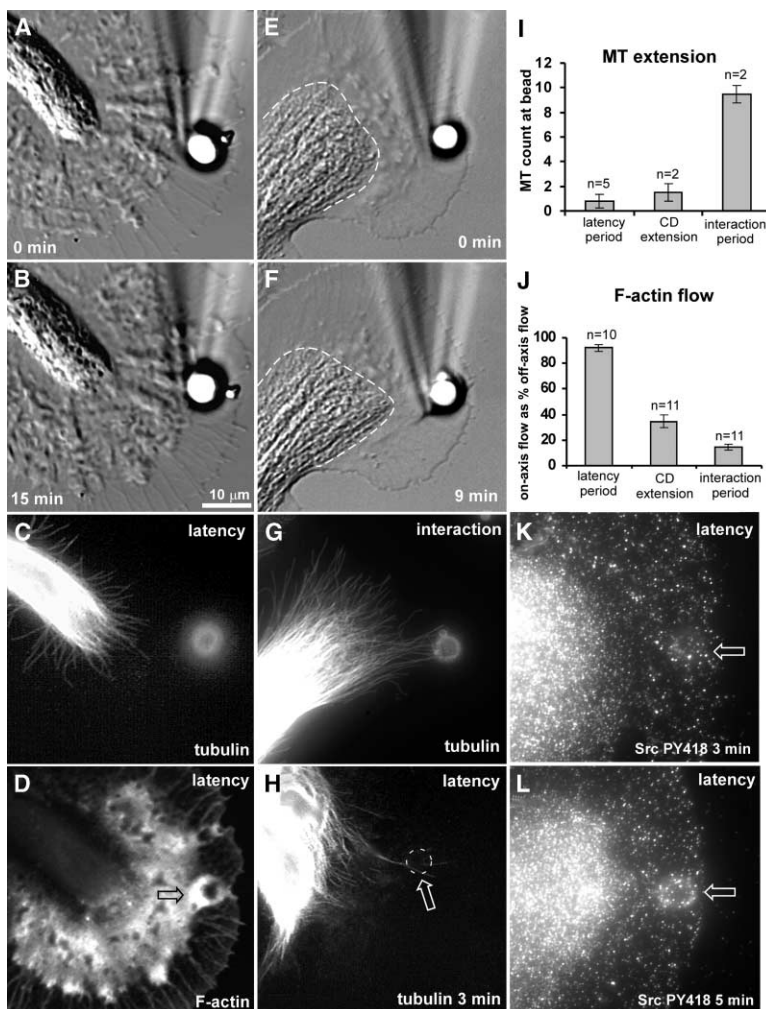


Figure 2. F-actin Accumulation and Src Activation Precede Net Microtubule Buildup, which Correlates with Attenuation of Retrograde Actin Flow

(A) DIC image of a growth cone right after placement of a bead coated with apCAM antibody (4E8). (B) The same growth cone 15 min later during the latency period (before C domain extension, tension increase, or leading edge growth). (C) Microtubule immunocytochemistry at the time point shown in (B). Diffuse bead labeling results from the detection of 4E8 by the secondary anti-mouse antibody. (D) F-actin accumulation around the bead (arrow). (E) Growth cone after 4E8 bead placement. (F) 1 min after start of interaction period. (G) Microtubule labeling during interaction period at time point in (F) reveals ~9 microtubules at bead. (H) Another example during the latency period shows two microtubules at the bead (marked with a dashed circle). (I) Microtubule number at beads during different phases of RBIs. Mean values \pm SEM; n = number of experiments. (J) F-actin flow measurements using marker beads both along RBI axis (on-axis flow; Figure 3H) and outside axis (off-axis flow; Figure 3I) and graphed as on-axis flow rate normalized by off-axis flow. Mean values \pm SEM. (K and L) Activated Src family kinase distribution (using Src PY418 antibody) in growth cones fixed 3 and 5 min into the latency period. Arrows denote bead positions.

previously characterized phosphospecific antibody that recognizes the autophosphorylation site PY418 of activated Src family kinases [17], active Src around restrained beads was increased by more than 100% within 5 min (Figures 2K and 2L, cf. Figure 4J for quantification). In summary, actin assembly and active Src accumulation appear to be early local events at bead target sites during the latency period, whereas microtubules likely explore target sites multiple times during a typical latency but do not accumulate during this time.

Dynamic Microtubules Are Necessary for apCAM-Mediated Target Interactions

We previously reported that C domain advance is correlated with slowing of retrograde actin flow during the target interaction phase [16, 18]; however, the mechanism of microtubule advance is unknown. When RBIs were halted by fixation during the interaction period (i.e., after the start of C domain advance), microtubule extension was typically already evident (Figures 2E–2G). Since under the control conditions microtubules are transported rearward by retrograde actin flow at about the same rate as they assemble [2], we wanted to test whether microtubules advance during target interactions as a result of continued assembly combined with

attenuation of actin flow (and microtubule transport) in the target interaction axis [16]. To address this, we first compared microtubule densities at target sites with retrograde actin flow rates: (1) during the latency period, (2) at the onset of C domain advance, and (3) during the interaction period (Figures 2I and 2J). Retrograde actin flow rates were determined using the laser trap assisted flow coupled bead assay (see Experimental Procedures and Figure 3) [18]. During the latency period, microtubule density at bead sites remained low and retrograde flow rates within the target interaction axis remained high ($\geq 90\%$ of control flow rates assessed adjacent to the bead binding site). In contrast, retrograde flow had slowed significantly by the onset of C domain extension with a corresponding slight increase in microtubule density. However, during the interaction phase, microtubule density at target sites increased dramatically and retrograde actin flow rates slowed maximally to 15% of control flow rates ($p < 0.001$). Thus, microtubule advance is well correlated with slowing of retrograde F-actin flow rates within the target interaction axis.

Next, we addressed whether target site-directed microtubule extension depends on microtubule assembly. Growth cones were first tested for RBI competence under control conditions using beads derivatized with re-

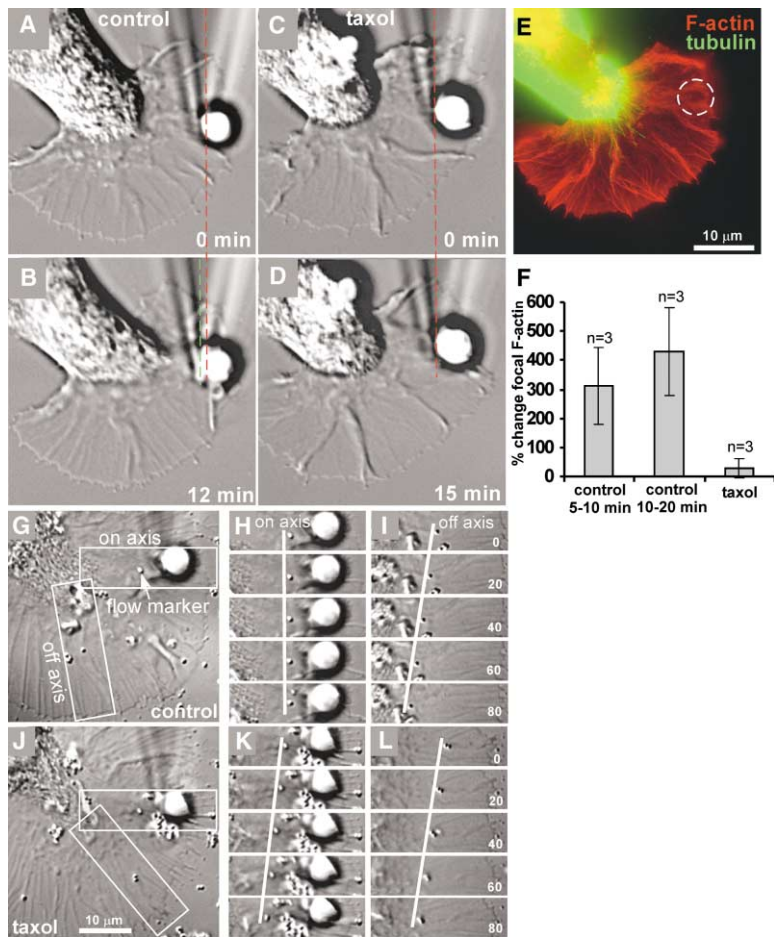


Figure 3. Dynamic Microtubules Are Required for All Key Aspects of Growth Cone Steering

(A and B) Control RBI using a bead coated with recombinant apCAM right after bead placement (A) and after C domain extension (B).

(C and D) Same growth cone after treatment with 100 nM taxol for 20 min, after bead placement (C), and after 15 min of bead restraint (D). Note absence of C domain extension, growth of the leading edge in front of the bead, and tension buildup (deflection of needle from red to green marker line).

(E) Fixation and labeling at 15 min shows no microtubules (green) extending to bead and no actin filament (red) accumulation (white circle = bead position).

(F) Relative focal F actin changes at beads during latency (5–10 min) and interaction (10–20 min) periods and in taxol-blocked RBIs.

(G–L) Microtubule dynamics are essential for strong apCAM-actin filament coupling.

(G–I) Control RBI with apCAM bead.

(G) Overview at start of interaction.

(H and I) Time-lapse montages of regions indicated at same time intervals. On-axis flow in this experiment was 1.03 $\mu\text{m}/\text{min}$ (H); off-axis flow was 4.63 $\mu\text{m}/\text{min}$ (I).

(J–L) The same growth cone after treatment with 100 nM taxol.

(J) Overview.

(K and L) Time-lapse montages showing that on-axis retrograde flow in taxol (3.83 $\mu\text{m}/\text{min}$; K) was only reduced by 16% compared to off-axis flow (4.58 $\mu\text{m}/\text{min}$; L). Time in (I) and (L) in seconds.

Supplemental Movie 4 shows a control RBI before taxol treatment, taken from (A) and (B). Supplemental Movie 5 shows the same growth as in Movie 4 after treatment with 100 nM taxol, taken from (C) and (D).

combinant apCAM (Figures 3A and 3B) and then challenged with a second bead in the presence of low doses of taxol (Figures 3C–3E) or vinblastine (Supplemental Figures S2C–S2E). Interestingly, dampening microtubule dynamics by either method inhibited all key characteristics of target interactions without marked effects on growth cone motility (Supplemental Movies 4 and 5). Site-directed F actin assembly around restrained beads, C domain extension, directed microtubule extension, and protrusive leading edge growth near interaction sites no longer occurred ($n = 5$; Figures 3C–3E; focal F actin quantifications, Figure 3F). In addition, the late tension increases typical of control RBIs and indicated by needle deflections were not observed (lines in Figures 3A–3D; Supplemental Figure S2). Interaction probability was reduced by 82% and 100% in taxol ($n = 11$) and vinblastine ($n = 7$), respectively.

We also noted that retrograde actin flow did not appear to slow within the target interaction axis in the presence of taxol (Supplemental Movie 5) or vinblastine, suggesting a role for microtubule dynamics in regulation of apCAM-actin filament coupling. To address this further, we compared actin flow rates within the interaction axis (on-axis) with flow in adjacent lamellipodium sec-

tors (off-axis) before and after taxol treatment (Figures 3G–3L). Under control conditions, strong attenuation of on-axis retrograde flow rates occurred during interactions (Figures 3H versus 3I) as previously described [16], whereas, in taxol, on-axis flow rates were only slightly reduced relative to off-axis rates (Figures 3K versus 3L). Note that retrograde flow rates observed in taxol were similar to off-axis flow rates observed under control conditions (Figure 1E). Similar results were observed in RBIs blocked by vinblastine (data not shown). These results suggest that dynamic microtubules are not essential for actin-based lamellar motility but play a more specialized signal transduction role in regulating apCAM interactions with the actin filament retrograde flow system [19].

Normal Src Function Requires Dynamic Microtubules

Under control conditions, activated Src accumulates along with F actin around restrained apCAM bead targets, and when Src activity is inhibited, beads no longer strongly couple to the underlying actin flow [17]. This behavior resembles the effects of dampening microtubule dynamics reported above (Figure 3) and prompted

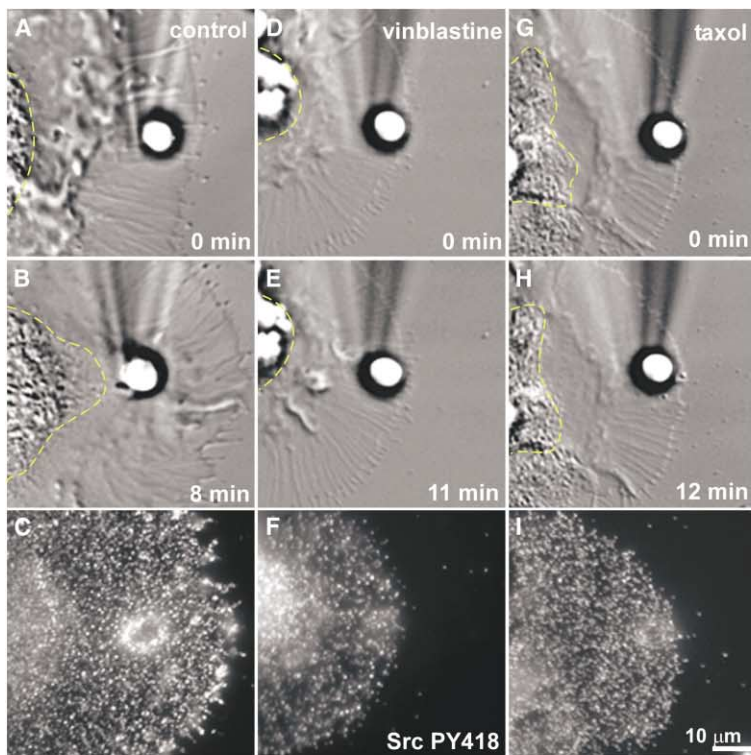


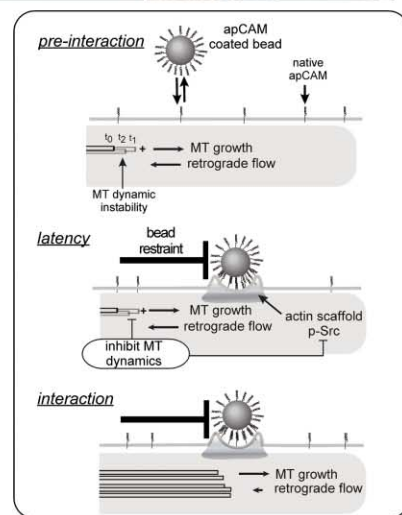
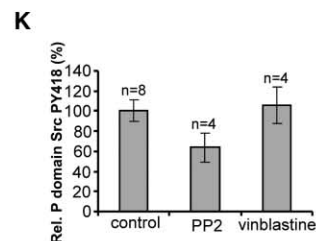
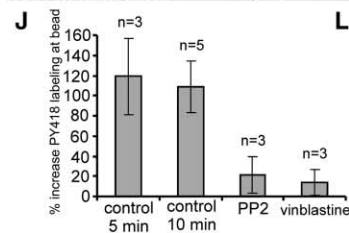
Figure 4. Microtubule Dynamics Are Necessary for Normal Src Family Kinase Function at Target Sites

(A–I) Control RBI experiment with 4E8 bead (A–C), RBI blocked by 25 nM vinblastine (D–F), and RBI blocked by 100 nM taxol (G–I). Upper row (A, D, and G) shows growth cones at start of experiment. Middle row (B, E, and H) shows time points when interaction was completed in controls (B), or when beads were restrained in the presence of the drugs (E and H) for at least the corresponding control latency and interaction time periods. C domain boundary indicated with yellow dashed lines. Bottom row (C, F, and I) shows immunolocalization of activated Src family kinases using the Src PY418 antibody.

(J) Quantification of % Src PY418 labeling increase at bead sites in control and in the presence of the Src family inhibitor PP2 (25 μ M) or vinblastine (25 nM).

(K) Average intensity of Src PY418 labeling in the P domain after \sim 30 min PP2 or vinblastine treatment plotted relative to controls. Mean values \pm SEM; n = number of experiments.

(L) Model (see text).



us to investigate a possible relationship between microtubule dynamics and Src function (Figure 4). Localization of active Src family kinase was assessed with the Src PY418 antibody during apCAM-mediated RBIs, and increased levels of Src PY418 were detected around 4E8-coated beads in controls (Figures 4A–4C) as reported. To investigate a possible role for microtubule dynamics in Src signaling, growth cones were first tested for interaction competence and then treated with low doses of vinblastine (Figures 4D–4F) or taxol (Figures 4G–4I) and challenged with a second target bead. Dampening of microtubule dynamics with vinblastine or taxol inhibited target interactions as above and also strongly suppressed accumulation of activated Src around bead targets (Figures 4F, 4I, and 4J). Note that Src family kinase

inhibitor PP2 also inhibits apCAM bead target interactions and suppresses focal accumulation of active Src (Figure 4J) [17]; however, there are some important differences. Whereas treatment with PP2 (25 μ M) reduced average Src activity in the P domain by 36% as expected (Figure 4K; $p < 0.05$), vinblastine (25 nM) treatment had no effect on average Src activity (Figure 4K; $p = 0.4$) and affected Src accumulation only at target sites (Figures 4F and 4I). These results suggest that dynamic microtubules play a role in accumulation of active Src at target contact sites but are not necessary for maintaining Src activity per se. Possible scenarios could involve microtubule-dependent delivery or activation of Src itself, a Src docking protein, or factors that could potentiate Src activity at target sites. The latter would

include membrane components since local insertion of new membrane at the growth cone appears to depend critically on dynamic microtubules [20].

A model summarizing the above effects is shown in Figure 4L. Before a target interaction (Figure 4L, pre-interaction phase), native apCAM is freely diffusible and microtubules explore the P domain by periods of growth, pause, and shrinkage, i.e., the classic properties of microtubule dynamic instability (Figure 4L, t_0 , t_1 , t_2 are successive microtubule positions). Interestingly, maximum rates of microtubule growth ($\sim 7 \mu\text{m}/\text{min}$) are only slightly greater than the constant rate of retrograde actin flow. Since microtubule assembly rates fluctuate stochastically, this results in a steady state where microtubules transiently explore the P domain during periods of growth by "beating retrograde actin flow" and are cleared from the periphery whenever they pause by coupling to retrograde flow [2]. This results in rapid turnover, but little or no accumulation of, microtubules in the P domain in the absence of a target substrate. This pattern of constant microtubule exploration persists during the latency phase, during which time restrained apCAM-coated beads can also trigger assembly of an actin filament structure around the target bead. This may act as a scaffold for localized recruitment of active Src (P-src) and possibly other cell adhesion and signaling components. Importantly, inhibition of microtubule dynamics prevents both formation of the actin scaffold and active Src accumulation, suggesting that microtubule dynamics supports a step upstream of these early events in the target interaction sequence. Finally, during the interaction phase, retrograde actin flow attenuation is observed and microtubules extend toward the target site, likely because the average rate of microtubule assembly now exceeds opposing retrograde actin flow. Microtubule assembly is clearly necessary for microtubule advance, since low doses of taxol or vinblastine completely blocked microtubule extension during target interactions (Figure 3). These results do not, however, rule out a potential role for molecular motors in the microtubule extension process and bears further investigation. The current work compliments previous findings that dynamic microtubules are not essential for growth cone motility but play a higher-level role that enables discrimination of molecular guidance cues.

Supplemental Data

Supplemental Data including Experimental Procedures, figures, and movies are available at <http://www.current-biology.com/cgi/content/full/14/13/1194/DC1>.

Acknowledgments

The authors thank Dr. E. Kandel (Columbia University, NY) for providing the 4E8 monoclonal antibody. We are indebted to Dr. Tracy Cao, Dr. Mark Mooseker, Doris Kemler, and Nadia Ruthardt for technical advice and assistance in production of recombinant apCAM using the *Baculovirus* expression system. We further thank Dr. Laurie Iten (Purdue University, IN) for help with digital movies.

Received: November 24, 2003

Revised: May 24, 2004

Accepted: May 24, 2004

Published: July 13, 2004

References

1. Tanaka, E.M., and Kirschner, M.W. (1991). Microtubule behavior in the growth cones of living neurons during axon elongation. *J. Cell Biol.* 115, 345–363.
2. Schaefer, A.W., Kabir, N., and Forscher, P. (2002). Filopodia and actin arcs guide the assembly and transport of two populations of microtubules with unique dynamic parameters in neuronal growth cones. *J. Cell Biol.* 158, 139–152.
3. Tanaka, E., Ho, T., and Kirschner, M.W. (1995). The role of microtubule dynamics in growth cone motility and axonal growth. *J. Cell Biol.* 128, 139–155.
4. Williamson, T., Gordon-Weeks, P.R., Schachner, M., and Taylor, J. (1996). Microtubule reorganization is obligatory for growth cone turning. *Proc. Natl. Acad. Sci. USA* 93, 15221–15226.
5. Challacombe, J.F., Snow, D.M., and Letourneau, P.C. (1997). Dynamic microtubule ends are required for growth cone turning to avoid an inhibitory guidance cue. *J. Neurosci.* 17, 3085–3095.
6. Buck, K.B., and Zheng, J.Q. (2002). Growth cone turning induced by direct local modification of microtubule dynamics. *J. Neurosci.* 22, 9358–9367.
7. Sabry, J.H., O'Connor, T.P., Evans, L., Toroian-Raymond, A., Kirschner, M., and Bentley, D. (1991). Microtubule behavior during guidance of pioneer neuron growth cones in situ. *J. Cell Biol.* 115, 381–395.
8. Lin, C.H., and Forscher, P. (1993). Cytoskeletal remodeling during growth cone-target interactions. *J. Cell Biol.* 121, 1369–1383.
9. Tanaka, E., and Sabry, J. (1995). Making the connection: cytoskeletal rearrangements during growth cone guidance. *Cell* 83, 171–176.
10. Dent, E.W., and Kalil, K. (2001). Axon branching requires interactions between dynamic microtubules and actin filaments. *J. Neurosci.* 21, 9757–9769.
11. Zhou, F.Q., Waterman-Storer, C.M., and Cohan, C.S. (2002). Focal loss of actin bundles causes microtubule redistribution and growth cone turning. *J. Cell Biol.* 157, 839–849.
12. Jordan, M.A., and Wilson, L. (1998). Use of drugs to study role of microtubule assembly dynamics in living cells. *Methods Enzymol.* 298, 252–276.
13. Kirschner, M., and Mitchison, T. (1986). Beyond self-assembly: from microtubules to morphogenesis. *Cell* 45, 329–342.
14. Kaverina, I., Rottner, K., and Small, J.V. (1998). Targeting, capture, and stabilization of microtubules at early focal adhesions. *J. Cell Biol.* 142, 181–190.
15. Kaverina, I., Krylyshkina, O., and Small, J.V. (1999). Microtubule targeting of substrate contacts promotes their relaxation and dissociation. *J. Cell Biol.* 146, 1033–1044.
16. Suter, D.M., Errante, L.D., Belotserkovsky, V., and Forscher, P. (1998). The Ig superfamily cell adhesion molecule, apCAM, mediates growth cone steering by substrate-cytoskeletal coupling. *J. Cell Biol.* 141, 227–240.
17. Suter, D.M., and Forscher, P. (2001). Transmission of growth cone traction force through apCAM-cytoskeletal linkages is regulated by Src family tyrosine kinase activity. *J. Cell Biol.* 155, 427–438.
18. Lin, C.H., and Forscher, P. (1995). Growth cone advance is inversely proportional to retrograde F-actin flow. *Neuron* 14, 763–771.
19. Rodriguez, O.C., Schaefer, A.W., Mandato, C.A., Forscher, P., Bement, W.M., and Waterman-Storer, C.M. (2003). Conserved microtubule-actin interactions in cell movement and morphogenesis. *Nat. Cell Biol.* 5, 599–609.
20. Zakharenko, S., and Popov, S. (1998). Dynamics of axonal microtubules regulate the topology of new membrane insertion into the growing neurites. *J. Cell Biol.* 143, 1077–1086.

Microtubule Dynamics Are Necessary for Src Family Kinase-Dependent Growth Cone Steering

Daniel M. Suter, Andrew W. Schaefer,
and Paul Forscher

Supplemental Results

Recombinant apCAM-Coated Beads Induce Growth Cone Steering

We have previously shown that apCAM-specific ligands, such as the monoclonal antibody 4E8 and apCAM protein purified from *Aplysia* nervous system, support growth cone steering events when presented on silica beads using the RBI assay (Suter et al., 1998). To have ready access to purified protein, we cloned the extracellular portion of apCAM into a baculovirus expression vector. Supplemental Figure S1 shows SDS-PAGE and Western blot characterization of the recombinant His-tagged apCAM after Ni-NTA purification. The molecular weight (100 kDa) of the purified recombinant apCAM is similar to that reported for GPI-linked isoforms of apCAM (Mayford et al., 1992). When Ni-NTA beads were coated with His-apCAM and used in the RBI assay, we observed growth cone steering events (Figures S1B and S1C) similar to those reported for beads coated with 4E8 or native apCAM (Suter et al., 1998). The clearest indicator of a successful RBI under differential interference contrast (DIC) observation is acute extension of the C domain toward the bead (Figure S1C). Quantification of RBI experiments using recombinant apCAM is given in Figure S1D. RBI probability for His-apCAM (72%) was similar to tissue-purified protein (68%; Suter et al., 1998). These interactions were inhibited by addition of 4E8 antibody to levels similar to untreated control beads. RBI experiments reported in this paper were carried out with both recombinant His-apCAM and 4E8-coated beads with similar efficacy.

Supplemental Experimental Procedures

Recombinant apCAM

A baculovirus expression system from Life Technologies was used to produce recombinant apCAM protein comprising the extracellular portion plus a C-terminal His-tag. Briefly, the sense primer 5'-TTAG CGCGCCACCATGGATTTTGCTTACATAAT TTTTGTGGC-3' (BssH II site underlined) and the antisense primer 5'-ATTATACTAGT TGT TAGCAGCCGGATCTCAGTGG-3' (SpeI site underlined) plus Pfx polymerase (Invitrogen) was used to amplify the complete extracellular part of apCAM from a His-tagged apCAM clone in pet21a vector (Novagen). This template was previously cloned from the d19 apCAM clone (transmembrane isoform) in pNEX δ vector (kindly provided by the laboratory of Dr. E. Kandel, Columbia University, NY) [S1] into the pet21a vector. The PCR product was cloned into pFastBacDUAL using the BssH II and SpeI sites and verified by sequencing. DH10Bac bacteria were transformed with pFastBacDUAL vector containing the apCAM insert to produce bacmid DNA for transfection of SF9 insect cells. Conditioned medium as well as SF9 cells were harvested from the second round of viral infections as a source for His-tag purification of recombinant apCAM using Nickel-NTA beads according to manufacturer's instructions. The purified protein was dialyzed against PBS, and protein concentration was determined with the BCA assay (Pierce Chemical Co.). Recombinant apCAM was analyzed by 7.5% SDS-PAGE followed by silver staining and by immunoblotting using either 0.5 μ g/ml apCAM-specific monoclonal antibody 4E8 [S2] or 0.2 μ g/ml His-tag antibody (BABC0). After incubation with secondary goat anti-mouse POD antibody at 0.2 μ g/ml (Pierce), detection was carried out with the ECL method according to the manufacturer's instructions (Amersham Pharmacia Biotech).

Bead Preparation and Bead Assays

Beads for RBI experiments were prepared either by coating 5 μ m silica Ni-NTA beads (Micromod) with purified recombinant apCAM

or by covalently linking purified 4E8 antibody to glutaraldehyde-activated 5 μ m silica amino beads (Bangs Laboratories). NTA silica beads were charged at 5% (w/v) with 0.1 M NiSO₄ for 30 min, followed by two washes with H₂O and two washes with PBS. Beads were then incubated at 1% (w/v) with purified apCAM (300 μ g/ml in PBS) o.n. at 4°C. Residual sites were blocked with 5 mg/ml BSA in PBS for 30 min at RT. Beads were stored in ligand solution and washed twice with PBS before RBI experiments. Glutaraldehyde activation of 5 μ m silica amino beads was carried out as previously described [S3]. 1 mg/ml purified 4E8 in PBS was coupled to 1% (w/v) beads o.n. at 4°C. 5 mg/ml BSA in 50 mM Tris (pH 8.0) was used to backfill any residual active sites. Beads were stored in blocking solution and washed twice with PBS before experiments. The RBI assay was carried out as reported [S4]. 500 nm silica beads (Bangs Laboratories) were coated with Con A [S4] or polyethylenimine [S5] and placed on the growth cone peripheral domain with an infrared laser trap to measure retrograde actin flow rates [S6].

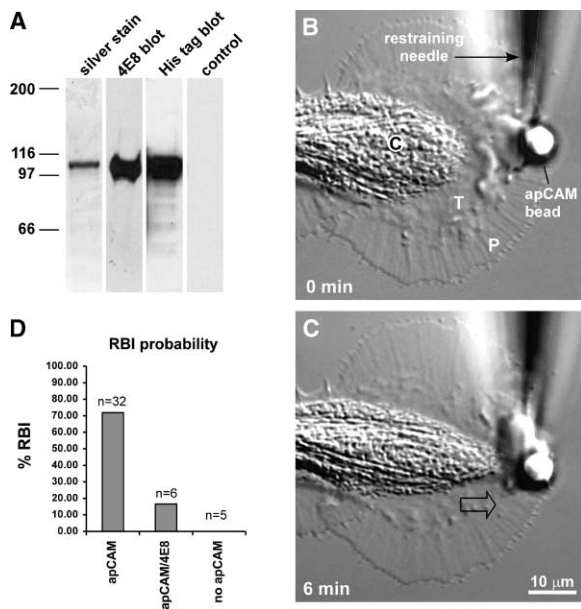


Figure S1. Recombinant apCAM Induces RBIs

(A) Characterization of the baculovirus-expressed extracellular portion of apCAM by SDS-PAGE and silver staining (lane 1), Western blot detection with 4E8 antibody (lane 2), His-tag antibody (lane 3), and no primary antibody control (lane 4). A single band was detected at 100 kDa.

(B) DIC image of an *Aplysia* neuronal growth cone at start of an RBI experiment using a bead coated with recombinant apCAM. Peripheral (P) and central (C) cytoplasmic domains and transition zone (T) are indicated.

(C) C domain extended toward restrained bead (arrow). Scale bar equals 10 μ m.

(D) Statistics of RBI probability with recombinant apCAM beads plotted as % of successful interactions per total number of experiments. Controls: apCAM beads in the presence of excess amounts of 4E8 antibody or beads with no apCAM. n indicates the number of experiments.

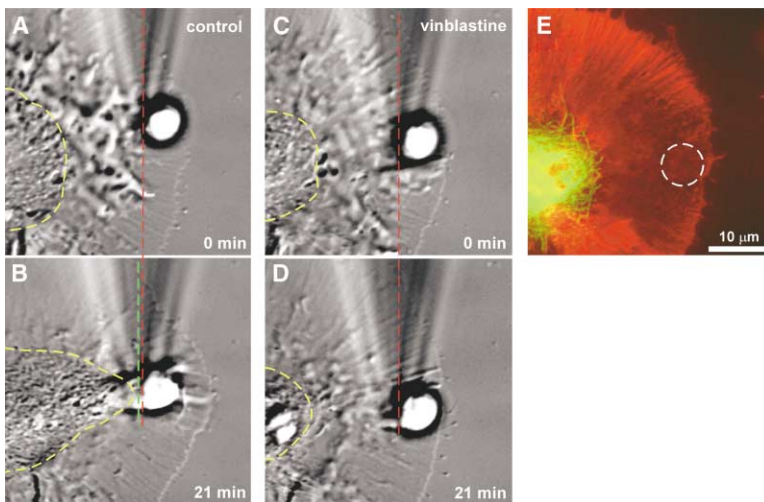


Figure S2. Vinblastine Inhibits RBIs

(A and B) Control RBI with apCAM bead. (C and D) Same growth cone after treatment with 25 nM vinblastine for 20 min, after bead placement (C), and 21 min later (D). (E) No microtubules (green) near, and no actin filament (red) accumulation around bead site (white dashed circle). As in taxol, all RBI characteristics are absent after vinblastine treatment.

Cell Culture

Aplysia bag cell neurons were cultured on polylysine-coated coverslips in L15 medium (Life Technologies, Frederick, MD) supplemented with artificial seawater (ASW) as previously described [S4, S7]. During experiments involving application of beads, the medium was supplemented with 5 mg/ml BSA to block nonspecific bead binding.

Video-Light Microscopy and Image Processing

Video-enhanced differential interference contrast (DIC) time-lapse and fluorescence microscopy were performed as described [S4, S7, S8]. DIC images were captured every 10 s. A 151-AT series image processor (Imaging Technology Inc.) was used for real-time video image processing, image analysis using custom-written software, and image digitization for export into Photoshop 7.0 (Adobe) for image processing. The majority of fluorescence images were taken with a Photometrics CoolSNAP Fx cooled CCD camera (Roper Scientific) on an Eclipse 300 (Nikon) inverted microscope controlled by Metamorph 4.0 imaging software (Universal Imaging). The same software was used for making montages of time-lapse sequences and quantification of fluorescence intensities.

Microtubule Inhibitor Experiments

Taxol and vinblastine (Sigma) stock solutions of 1 mM were prepared in DMSO and H₂O, respectively. In all experiments involving inhibitors, a red long pass filter (590 nm cut on) was used for DIC time-lapse recording. Bag cell growth cones were observed first under control conditions (medium plus DMSO in the case of taxol), then treated for 20 min with inhibitors. During this period, exposure to light was kept to a minimum to avoid potential phototoxic effects. The same experimental paradigm was used to assess microtubule assembly inhibitor effects in the RBI assay. Only growth cones that had successfully interacted with the bead under control conditions were treated with drug for 20 min and then reassessed for RBI capability. Beads were restrained in the presence of microtubule inhibitors for at least 150% of the control latency time. (Latency period is operationally defined as the interval between bead placement and observable advance of the central cytoplasmic domain [S4].)

Fluorescence Labeling and Quantification

Bag cell neurons were fixed by rapid exchange of the medium with 3.7% formaldehyde in ASW supplemented with 400 mM sucrose. After fixation for 30 min, the cells were permeabilized for 10 min using 1% triton X-100 in the fixation solution. Cells were then washed three times with PBS containing 0.1% triton X-100 (wash solution). For actin filament double labeling, Alexa 488-phalloidin (Molecular Probes) was incubated at 1 unit/ml in wash solution for 15 min. After three washes, the cells were blocked with 5% BSA in wash solution

for 30 min and incubated with the mouse anti- β -tubulin antibody (Sigma) at 5 μ g/ml in blocking solution for 1 hr at RT. After three washes, Alexa 568 goat anti-mouse IgG (Molecular Probes) was added at 20 μ g/ml in blocking solution for 30 min at RT. The final wash solution was replaced with antifading solution (20 mM n-propyl-gallate (Sigma) in 80% glycerol/20% PBS [pH 8.5]) before fluorescence inspection. Src PY418 labeling using the phosphospecific rabbit antibody from Biosource International was carried out as recently described [S9]. To determine Src PY418 and F actin levels at bead-growth cone interaction sites, the average fluorescence intensity in 3 μ m² square areas distributed over the bead interaction sites was obtained using the Metamorph region tools. After background subtraction, this value was normalized against the average fluorescence intensity of the peripheral domain surrounding the interaction site. Average increase in percentage was determined for at least three experiments per condition.

Analysis of Microtubule Dynamics Using Multimode FSM

DIC and fluorescence speckle microscopy (FSM) was carried out as recently described [S10] using 1 mg/ml Alexa-594-conjugated tubulin in injection buffer (100 mM PIPES, 1 mM MgCl₂, 1 mM EGTA). After the cells were allowed to recover for 1 hr, images of labeled microtubules and corresponding DIC pictures were taken every 10 s with a Quantix 57 back illuminated frame transfer camera (Roper Scientific). Image processing and analysis using Metamorph software was done as reported [S10].

Supplemental References

- S1. Bailey, C.H., Kaang, B.K., Chen, M., Martin, K.C., Lim, C.S., Casadio, A., and Kandel, E.R. (1997). Mutation in the phosphorylation sites of MAP kinase blocks learning-related internalization of apCAM in *Aplysia* sensory neurons. *Neuron* 18, 913–924.
- S2. Keller, F., and Schacher, S. (1990). Neuron-specific membrane glycoproteins promoting neurite fasciculation in *Aplysia californica*. *J. Cell Biol.* 111, 2637–2650.
- S3. Thompson, C., Lin, C.H., and Forscher, P. (1996). An *Aplysia* cell adhesion molecule associated with site-directed actin filament assembly in neuronal growth cones. *J. Cell Sci.* 109, 2843–2854.
- S4. Suter, D.M., Errante, L.D., Belotserkovsky, V., and Forscher, P. (1998). The Ig superfamily cell adhesion molecule, apCAM, mediates growth cone steering by substrate-cytoskeletal coupling. *J. Cell Biol.* 141, 227–240.
- S5. Forscher, P., Lin, C.H., and Thompson, C. (1992). Novel form of growth cone motility involving site-directed actin filament assembly. *Nature* 357, 515–518.

- S6. Lin, C.H., and Forscher, P. (1995). Growth cone advance is inversely proportional to retrograde F-actin flow. *Neuron* *14*, 763–771.
- S7. Forscher, P., and Smith, S.J. (1988). Actions of cytochalasins on the organization of actin filaments and microtubules in a neuronal growth cone. *J. Cell Biol.* *107*, 1505–1516.
- S8. Lin, C.H., and Forscher, P. (1993). Cytoskeletal remodeling during growth cone-target interactions. *J. Cell Biol.* *121*, 1369–1383.
- S9. Suter, D.M., and Forscher, P. (2001). Transmission of growth cone traction force through apCAM-cytoskeletal linkages is regulated by Src family tyrosine kinase activity. *J. Cell Biol.* *155*, 427–438.
- S10. Schaefer, A.W., Kabir, N., and Forscher, P. (2002). Filopodia and actin arcs guide the assembly and transport of two populations of microtubules with unique dynamic parameters in neuronal growth cones. *J. Cell Biol.* *158*, 139–152.